Published in final edited form as:
AJR Am J Roentgenol. 2013 January ; 200(1): 177–183. doi:10.2214/AJR.12.8996.

Characterization of Human Brown Adipose Tissue by Chemical-Shift Water-Fat MRI

Houchun H. Hu[1], **Thomas G. Perkins**[2], **Jonathan M. Chia**[2], and **Vicente Gilsanz**[1]

[1]Department of Radiology, Children's Hospital Los Angeles, 4650 Sunset Blvd, MS #81, Los Angeles, California 90027

[2]Philips Healthcare, Cleveland, Ohio

Abstract

OBJECTIVE—The purpose of this study was to characterize human brown adipose tissue (BAT) with chemical-shift water-fat MRI and to determine whether trends and differences in fat-signal fractions and T2* relaxation times between BAT and white adipose tissue (WAT) are consistently observed postmortem and in vivo in infants, adolescents, and adults.

MATERIALS AND METHODS—A postmortem body and eight patients were studied. A six-echo spoiled gradient-echo chemical-shift water-fat MRI sequence was performed at 3 T to jointly quantify fat-signal fraction and T2* in interscapular-supraclavicular BAT and subcutaneous WAT. To confirm BAT identity, biopsy and histology served as the reference in the postmortem study and PET/CT was used in five of the eight patients who required examination for medical care.

RESULTS—Fat-signal fractions and T2* times were lower in BAT than in WAT in the postmortem example and in seven of eight patients. With the exception of one case, nominal comparisons between brown and white adipose tissues were statistically significant ($p < 0.05$). Between subjects, a large range of fat-signal fraction values was observed in BAT but not in WAT.

CONCLUSION—We have shown that fat-signal fractions and T2* values jointly derived from chemical-shift water-fat MRI are lower in BAT than in WAT likely because of differences in cellular structures, triglyceride content, and vascularization. The two metrics can serve as complementary biomarkers in the detection of BAT.

Keywords

brown adipose tissue; chemical-shift water-fat MRI; fat fraction; T2* relaxation; white adipose tissue

Bown adipose tissue (BAT) is responsible for thermogenesis, and many reports have investigated BAT physiology in animals [1–4]. More recently, the discovery of human BAT with PET/CT has reinvigorated scientific interest, particularly in metabolism and obesity [5–8]. In contrast to white adipose tissue (WAT), which stores energy as triglycerides, BAT metabolizes fat to generate heat when stimulated. WAT is characterized by large adipocytes that contain a unilocular lipid droplet, a displaced peripheral nucleus, and limited cytoplasm. BAT contains smaller adipocytes with multiple intracellular lipid droplets, a centrally located nucleus, and an abundance of iron-rich mitochondria. BAT is also densely

Address correspondence to H. H. Hu (hhu@chla.usc.edu).
T. G. Perkins and J. M. Chia are employees of Philips Healthcare.

vascularized by capillaries needed to transport and disperse the produced heat. Whereas the detection of BAT by PET/CT is based on tissue function and radiotracer uptake, the intrinsic morphologic differences between BAT and WAT can give rise to unique signatures that can be detected by standalone CT [9] and MRI.

Thus, several recent works have shown the feasibility of using MRI to image BAT and have shown distinct signal contrast between BAT and WAT in mice. These approaches have exploited the aforementioned differences between BAT and WAT to identify unique spectral interactions [10]; fat-signal fractions [11]; T1 [12], T2, and T2* relaxation times [13–15]; triglyceride saturation [12]; and blood perfusion [14–16]. Collectively, these studies support quantitative MRI as a platform capable of detecting and characterizing BAT in vivo in humans, independent of the tissue's metabolic activity state. Because MRI does not use ionizing radiation and does not require an exogenous tracer to visualize BAT, the modality can be broadly used in healthy cohorts, including children.

Building on these prior studies and recent case reports [17, 18], we extended the investigation to infants, adolescents, and adult human subjects. On the basis of previous systematic findings in animals that fat-signal fractions and T2* differences manifest between BAT and WAT as a consequence of variations in intracellular fat, mitochondrial content, and blood perfusion between the two adipocytes, the purpose of this article was to determine whether such differences can be consistently observed in a postmortem body, infants, adolescents, and adults. A secondary goal was to show that the capability of chemical-shift water-fat MRI in jointly estimating fat-signal fraction and T2* metrics is advantageous in BAT imaging because the technique provides two independent but complementary mechanisms of signal contrast. We hypothesize that both the fat-signal fraction and the T2* values are lower in BAT than in WAT and that, although the absolute difference may vary between subjects and between a postmortem body versus an in vivo setting, such trends are nevertheless present regardless of underlying BAT metabolic activity.

Materials and Methods

Subjects

Local institutional review board approvals were obtained for this research. This study was HIPAA compliant. The study cohort for this work involved a postmortem body and eight patients, five of whom were referred from our institution's department of oncology. Recruitment for this pilot project was open to all eligible patients of all ages at our institution, and those who agreed to participate after initial recruitment were asked to further provide written informed consent. No eligible patient who gave consent was excluded from the study. Age and gender of the study cohort are summarized in Table 1, and these were not used as exclusion criteria. The postmortem body was studied first with MRI, followed by histologic analysis to confirm BAT findings. This procedure was performed to corroborate and reinforce previous findings from a literature case report [18]. The five oncology patients were studied with MRI on the same day after their clinically scheduled PET/CT examination. The remaining three pediatric patients were studied only with MRI as part of their standard of care and did not participate in any other procedures. For all MRI examinations, no sedation was used.

Chemical-Shift Water-Fat MRI

All MRI examinations were performed on a 3-T whole-body human platform (Achieva R3.2, Philips Healthcare) at a room (MRI suite) temperature of approximately 22°C. For the postmortem study, the body was imaged within 48 hours of death and was not frozen. A currently noncommercial version of the mDIXON (Philips Healthcare) chemical-shift water-

fat multiecho pulse sequence provided by the manufacturer was used [19, 20] as a research protocol at our institution. Imaging parameters and setup for the spoiled gradient-echo sequence are summarized in Table 2. Average scanning time was approximately 3–5 minutes. The sequence is a six-echo generalization of the traditional in-phase-opposed-phase two-echo Dixon water-fat imaging technique. Data reconstruction yields coregistered fat, water, in-phase, and out-of-phase image series; quantitative fat-signal fraction; and T2* maps [21]. The mDIXON postprocessing algorithm uses a seven-peak spectral model of fat previously obtained from high-resolution MR spectroscopy [22], and, when coupled with the use of a small flip angle to minimize T1 bias [23], the resultant fat-signal fraction maps accurately reflect the underlying proton density–ratios between fat and the sum of fat and water from a range of 0–100% [24, 25]. This type of multiecho water-fat sequence has been recently used to measure fat accumulation in liver [21, 25], pancreas [26], heart [27], skeletal muscle [28], and body adiposity [29]. As has been previously explained [21, 25], multiecho chemical-shift water-fat MRI jointly estimates fat-signal fraction and T2*, with the latter metric typically considered a confounding factor that needs to be accounted for to accurately separate water and fat signals and facilitate the computation of the former parameter.

Histology

To confirm BAT identity, tissue biopsy and histologic analysis were performed for the initial postmortem study. Tissue samples from interscapular BAT depots were extracted by a pathologist after reviewing the MR images with a pediatric radiologist. Extracted samples were fixed in formalin, embedded in paraffin, and stained with H and E for visual analysis under a microscope.

PET/CT

For the oncology patients, visual identification of interscapular and supraclavicular BAT was either positively (BAT+) or negatively (BAT−) confirmed by a radiologist after inspection of the PET/CT results in a manner similar to current practices reported in the literature [5–8]. All clinical PET/CT examinations were performed on a Gemini system (GXL, release 3.3, Philips Healthcare). Except for ^{18}F-FDG, no other agents were administered, nor were any of the patients subjected to cold and warm temperature preparations to stimulate or suppress BAT activity. Patients were not in a fasting state and were indoors under climate-controlled room temperature (22°C) for at least 1 hour before their examinations.

Data Analysis

Image analysis of fat-signal fraction and T2* maps generated from MRI was performed with SliceOmatic (Tomovision) to compute mean and SD values across adipose tissue depots. In each subject, regions of interest encompassing the interscapular and supraclavicular BAT depots and subcutaneous WAT were drawn on coregistered water and fat image series and transferred to the corresponding fat-signal fraction and T2* maps for quantification. The Student *t* test (StatView, version 5.0.1, SAS Institute) was used to assess differences in fat-signal fraction and T2* between BAT and WAT, using a criterion of $p < 0.05$.

Results

Postmortem Body

Figure 1 illustrates representative coronal MRI results from the postmortem body study. A reconstructed gray-scale water image and colorized quantitative fat-signal fraction and T2* maps are shown. The fat-signal fraction map is shown on a full color scale from 0 to 100%.

For illustration clarity, the T2* map is shown on a condensed scale from 0 to 26 ms, such that any voxel with a computed T2* value ≥ 26 ms (mostly muscle, fluids, and WAT) is shown in red. Note gross edema in this body and evidence of pleural effusion. Bilateral BAT depots are outlined, and subcutaneous WAT is highlighted by arrowheads. BAT is slightly hyperintense and has a granular appearance in comparison with WAT in the water image. BAT also has a noticeably lower-valued representation in the fat-signal fraction map in contrast with WAT. Similarly, BAT depots are characterized by lower values in the T2* maps.

Figure 2 illustrates corroborating results from histology. The white arrowheads point to distinct large unilocular WAT adipocytes. In contrast, the black arrows point to multilocular BAT adipocytes. Multiple fat vacuoles can be clearly visualized within the BAT adipocytes, whereas only a single lipid vacuole can be observed in each WAT cell. Note near the upper portion of the image that BAT and WAT adipocytes appear intermixed.

Patients

The top row of Figure 3 presents results from adolescent patient 2 (BAT+) in a layout similar to Figure 1. In place of the MRI water image, PET results are shown. Bilateral uptake of FDG radionuclide tracer by BAT can be clearly observed. In the accompanying MRI results, the lower fat-signal fraction and T2* values of BAT in comparison with WAT are particularly evident. The bottom row of Figure 3 illustrates results from adolescent patient 3 (BAT−). Note that in contrast to patient 2, the PET examination does not show any signs of bilateral FDG uptake by BAT. Nevertheless, corresponding data from MRI show similar BAT patterns of lower fat-signal fractions and T2* values in comparison with WAT, similar to the illustrations from patient 2. As represented in the MRI fat-signal fraction maps, BAT depots exhibit a more heterogeneous and granular appearance in contrast with lipid-rich WAT. In the T2* maps, the heterogeneous appearance of BAT is even more visually apparent.

Figure 4 illustrates results from adult patients 4 and 5. For this example, the fat-signal fraction and the T2* maps have been rescaled on the same color bar (nominal values of 0–100% and 0–100 ms). The scale selection is arbitrary and was chosen for illustration clarity. Noticeable differences in fat-signal fraction and T2* values can be observed between the outlined BAT depots of patient 4, who was BAT+, and patient 5, who was BAT− (PET results not shown). Note in particular that patient 4 is very lean and has no noticeable subcutaneous WAT in the illustrated coronal view. Note in contrast in patient 5, who is moderately overweight, that differences in fat-signal fraction and T2* between BAT and WAT are diminished and not visually evident. In other words, patient 5's BAT appears very WAT-like. Figure 5 highlights representative results from pediatric patient 6, consistently showing the lower BAT values in both fat-signal fraction and T2* and the high tissue contrast in comparison with WAT. Imaging results from patients 7 and 8 were similar.

Figure 6 illustrates a representative scatterplot of fat-signal fraction and T2* values of BAT and WAT from patient 2. This format of visualizing the data highlights the dual fat-signal fraction and T2* signal contrast between BAT and WAT from chemical-shift water-fat MRI. It is clear that BAT (gray circles) occupies a distribution with lower fat-signal fraction and T2* values than WAT, resulting in a mirrored L-shaped pattern. This pattern was consistently observed in all cases except in patient 5. Lastly, Table 1 summarizes fat-signal fraction and T2* measurements from the postmortem body and all patient cases. With the exception of patient 5, comparisons between BAT and WAT values were statistically significant ($p < 0.05$).

Discussion

In this article, we have extended the application of chemical-shift water-fat MRI to quantitatively characterize differences in fat-signal fractions and T2* relaxation times between BAT and WAT in humans. Findings support dual fat-signal fraction and T2* metrics as complementary biomarkers of signal contrast between human BAT and WAT in a postmortem and, consistently, in pediatric and adolescent subjects. Although the current study involved only nine (one postmortem, eight in vivo) case examples, the data trend is systematically observed. The intrinsically greater proportion of intracellular water- and iron-rich mitochondria in BAT, coupled with a high degree of blood perfusion and deoxyhemoglobin during tissue activity, likely contributes to the overall lower fat-signal fraction and T2* values in the tissue compared with WAT [14, 15].

Using histology as corroborating evidence in the postmortem case, we have shown the feasibility of imaging metabolically inactive BAT with MRI, a capability that is not feasible with PET/CT. Conversely, using PET as supporting evidence, we have shown the feasibility of imaging both metabolically active (in patients 1, 2, and 4 who were BAT+) and inactive BAT (in patients 3 and 5 who were BAT−) in vivo. Results from patient 3 specifically highlight the potential utility of MRI in identifying BAT, independent of the tissue's metabolic status, and support the notion that the visual absence of BAT FDG uptake does not necessarily imply tissue absence. Observations in patient 5 also suggest that inactive BAT can exhibit appearances similar to WAT, supporting the notion that, if unused, metabolically inactive BAT accumulates its intracellular lipid stores, thereby becoming more WAT-like [5]. It has also been reported that lipid droplets within brown adipocytes can vary in size, depending on the tissue's level of stimulation and activity [30, 31]. Additionally, results from adult patients 4 and 5 (Fig. 4) support the current notion that BAT is inversely associated with body mass index [4] because it is evident from the imaging results that patient 5 has a greater body habitus than patient 4.

Currently, PET/CT remains the accepted and preferred modality for investigating metabolically active BAT. The methodology has been adopted in numerous studies in recent years, predominantly in adults. However, data on BAT in pediatric populations are scarce. The limited number of BAT studies in children with PET/CT is partially due to associated risk of ionizing radiation, and ethical restriction of performing such examinations in healthy children. The inclusion of adolescent oncology patients with a diagnosis of disease instead of healthy volunteers in this study reflects this limitation but was unavoidable because of the need to provide BAT evidence from PET/CT. However, imaging results from pediatric patient 6 and additional data from patients 7 and 8 offer evidence that rapid 3D chemical-shift water-fat MRI is capable of characterizing BAT in pediatric patients without the need of sedation.

As an alternative modality, MRI thus represents the most appropriate platform to overcome the shortcomings of PET/CT in BAT imaging. In particular, the ability of MRI to longitudinally assess BAT alterations and changes in metabolic activity in response to pharmacologic stimulation is highly attractive. It is worth noting that clinically the incidental uptake of FDG by BAT is a confounder in diagnosis and that preventive measures, such as warm blankets and in some reports pharmacologic agents, have been used to suppress BAT activity [32, 33]. Lastly, tracer uptake by metabolically active BAT is sensitive to climate and anesthesia [34].

It is premature to speculate on the clinical significance of imaging BAT in routine radiology workflow and standard patient care. However, methodologic advances in MRI will likely be one of the driving forces toward progress in understanding human BAT physiology.

Emerging MRI techniques, such as chemical-shift water-fat, will facilitate clinical research studies to gain deeper knowledge of BAT, and consequent findings can potentially have significant long-term implications. Currently, obesity and its comorbidities are difficult to treat and are costly health care expenditures.

Childhood obesity is of particular concern because obese children are at a high risk of becoming obese adults. Recent studies have suggested evidence and biochemical links between BAT, WAT [35], and skeletal muscle recruitment and development [36–38]. Because BAT regulates thermogenesis [39] and energy expenditure, elucidating BAT associations with adiposity and muscle tone can lead to promising strategies aimed at facilitating the recruitment of brown adipocytes and in the preventive treatment of obesity during early stages of life. Furthermore, although the comorbidities associated with WAT are fairly well understood and continue to be studied (e.g., type 2 diabetes, organ steatosis, metabolic syndrome), establishing the relationships and potential benefits of BAT from fetal origins through infancy and adolescence and beyond adulthood remains to be thoroughly investigated. Accurate MRI measures of BAT can reveal whether the tissue is a novel, independent predictor of the risk for disease and a potential determinant of healthy phenotypes.

Finally, we recognize several technical limitations related to the chemical-shift water-fat MRI approach adapted in this article. Currently, only a single T2* value was estimated per imaging voxel. A direction of future work is to use a dual T2* model to estimate individually the relaxation of fat and water components [40]. This could elucidate whether it is the T2* of water or of fat that actually shortens in BAT versus WAT and potentially add yet another dimension of measurable difference between the two tissues. Another possible limitation is that we used a multipeak fat spectral model based on human WAT and bone marrow [22], the default setting in the mDIXON reconstruction algorithm. It has been indicated that triglyceride characteristics between BAT and WAT are slightly different, particularly in the degree of carbon unsaturation [12]. However, it is unlikely that such subtle variations will significantly affect resultant fat-signal fraction and T2* estimations.

The sensitivity and specificity of MRI in detecting human BAT have not been determined and will necessitate a significantly larger cohort. With chemical-shift water-fat MRI, potential false-positive results of BAT identification can be particularly sourced from WAT that is edematous because of partial volume effects and inadequate spatial resolution. Alternative MRI techniques that are not susceptible to partial volume effects for BAT detection have been described [10]. Thus, the detection limit of BAT by chemical-shift water-fat MRI remains to be investigated, and the technique may likely serve as only one of many pulse sequences that are needed to unambiguously identify and characterize BAT in vivo.

In conclusion, the intrinsic cellular differences between BAT and WAT adipocytes give rise to complementary fat-signal fraction and T2* signal contrast from chemical-shift MRI, which can be observed in varying degrees postmortem and in vivo. Observations from this article are consistent with previous findings in mice [11–15] and support a framework for expanding the potential use of MRI to assess human BAT systematically in healthy asymptomatic populations. Additional study is needed to validate whether the trends in BAT and WAT fat-signal fraction and T2* data are similarly observed as a function of anthropometry and physiologic factors (e.g., age, gender, body adiposity, disease status, nutrition, and metabolism).

Acknowledgments

We thank Holger Eggers from Philips Healthcare for technical support with MRI; Jason Tovar and Zdena Pavlova for assistance with biopsy and histology; and Michelle Smith, Nicole Warburton, Patricia Aggabao, Montre Koh, Lisa Villanueva, Mercedes Landaverde, and Julia Castro for administrative project assistance.

H. H. Hu was supported by National Institutes of Health grant NIDDK-K25DK087931 and Zumberge Fund from the Office of the Provost at the University of Southern California.

V. Gilsanz was supported by National Institutes of Health grant NIDDK-R21DK090778.

References

1. Cinti S. The role of brown adipose tissue in human obesity. Nutr Metab Cardiovasc Dis. 2006; 16:569–574. [PubMed: 17113764]
2. Nedergaard J, Bengtsson T, Cannon B. Unexpected evidence for active brown adipose tissue in adult humans. Am J Physiol Endocrinol Metab. 2007; 293:E444–E452. [PubMed: 17473055]
3. Enerbäck S. Human brown adipose tissue. Cell Metab. 2010; 11:248–252. [PubMed: 20374955]
4. Nedergaard J, Cannon B. The changed metabolic world with human brown adipose tissue: therapeutic visions. Cell Metab. 2010; 11:268–272. [PubMed: 20374959]
5. Baba S, Jacene HA, Engles JM, Honda H, Wahl RL. CT Hounsfield units of brown adipose tissue increase with activation: preclinical and clinical studies. J Nucl Med. 2010; 51:246–250. [PubMed: 20124047]
6. Lee P, Greenfield JR, Ho KK, Fulham MJ. A critical appraisal of the prevalence and metabolic significance of brown adipose tissue in adult humans. Am J Physiol Endocrinol Metab. 2010; 299:E601–E606. [PubMed: 20606075]
7. Lee P, Zhao JT, Swarbrick MM, et al. High prevalence of brown adipose tissue in adult humans. J Clin Endocrinol Metab. 2011; 96:2450–2455. [PubMed: 21613352]
8. Pfannenberg C, Werner MK, Ripkens S, et al. Impact of age on the relationships of brown adipose tissue with sex and adiposity in humans. Diabetes. 2010; 59:1789–1793. [PubMed: 20357363]
9. Hu HH, Chung SA, Nayak KS, Jackson HA, Gilsanz V. Differential computed tomographic attenuation of metabolically active and inactive adipose tissues: preliminary findings. J Comput Assist Tomogr. 2011; 35:65–71. [PubMed: 21245691]
10. Branca RT, Warren WS. In vivo brown adipose tissue detection and characterization using water-lipid intermolecular zero-quantum coherences. Magn Reson Med. 2011; 65:313–319. [PubMed: 20939093]
11. Hu HH, Smith DL Jr, Nayak KS, Goran MI, Nagy TR. Identification of brown adipose tissue in mice with fat-water IDEAL-MRI. J Magn Reson Imaging. 2010; 31:1195–1202. [PubMed: 20432356]
12. Hamilton G, Smith DL Jr, Bydder M, Nayak KS, Hu HH. MR properties of brown and white adipose tissues. J Magn Reson Imaging. 2011; 34:468–473. [PubMed: 21780237]
13. Hu HH, Hines CD, Smith DL, Reeder SB. Variations in T2* and fat content of murine brown and white adipose tissues by chemical-shift MRI. Magn Reson Imaging. 2012; 30:323–329. [PubMed: 22244539]
14. Khanna A, Branca RT. Detecting brown adipose tissue activity with BOLD MRI in mice. Magn Reson Med. 2012
15. Chen YI, Cypess AM, Sass CA, et al. Anatomical and functional assessment of brown adipose tissue by magnetic resonance imaging. Obesity (Silver Spring). 2012; 20:1519–1526. [PubMed: 22343821]
16. Sbarbati A, Cavallini I, Marzola P, Nicolato E, Osculati F. Contrast-enhanced MRI of brown adipose tissue after pharmacological stimulation. Magn Reson Med. 2006; 55:715–718. [PubMed: 16506160]
17. Carter BW, Schucany WG. Brown adipose tissue in a newborn. Proc Bayl Univ Med Cent. 2008; 21:328–330. [PubMed: 18628932]

18. Hu HH, Tovar JP, Pavlova Z, Smith ML, Gilsanz V. Unequivocal identification of brown adipose tissue in a human infant. J Magn Reson Imaging. 2012; 35:938–942. [PubMed: 22180228]
19. Eggers H, Brendel B, Duijndam A, Herigault G. Dual-echo Dixon imaging with flexible choice of echo times. Magn Reson Med. 2011; 65:96–107. [PubMed: 20860006]
20. Eggers H, Perkins TG, Hussain SM. Influence of spectral model and signal decay on hepatic fat fraction measurements at 3 T with dual-echo Dixon imaging. Proc Intl Soc Magn Reson Med. 2011; 19:573. (abstr).
21. Hines CD, Agni R, Roen C, et al. Validation of MRI biomarkers of hepatic steatosis in the presence of iron overload in the ob/ob mouse. J Magn Reson Imaging. 2012; 35:844–851. [PubMed: 22127834]
22. Ren J, Dimitrov I, Sherry AD, Malloy CR. Composition of adipose tissue and marrow fat in humans by ^{1}H NMR at 7 Tesla. J Lipid Res. 2008; 49:2055–2062. [PubMed: 18509197]
23. Liu CY, McKenzie CA, Yu H, Brittain JH, Reeder SB. Fat quantification with IDEAL gradient echo imaging correction of bias from T1 and noise. Magn Reson Med. 2007; 58:354–364. [PubMed: 17654578]
24. Bydder M, Yokoo T, Hamilton G, et al. Relaxation effects in the quantification of fat using gradient echo imaging. Magn Reson Imaging. 2008; 26:347–359. [PubMed: 18093781]
25. Reeder SB, Cruite I, Hamilton G, Sirlin CB. Quantitative assessment of liver fat with magnetic resonance imaging and spectroscopy. J Magn Reson Imaging. 2011; 34:729–749. [PubMed: 21928307]
26. Hu HH, Kim HW, Nayak KS, Goran MI. Comparison of fat-water MRI and single-voxel MRS in the assessment of hepatic and pancreatic fat fractions in humans. Obesity (Silver Spring). 2010; 18:841–847. [PubMed: 19834463]
27. Kellman P, Hernando D, Shah S, et al. Multiecho Dixon fat and water separation method for detecting fibrofatty infiltration in the myocardium. Magn Reson Med. 2009; 61:215–221. [PubMed: 19097213]
28. Karampinos DC, Yu H, Shimakawa A, Link TM, Majumdar S. T1-corrected fat quantification using chemical shift-based water/fat separation: application to skeletal muscle. Magn Reson Med. 2011; 66:1312–1326. [PubMed: 21452279]
29. Alabousi A, Al-Attar S, Joy TR, Hegele RA, McKenzie CA. Evaluation of adipose tissue volume quantification with IDEAL fat-water separation. J Magn Reson Imaging. 2011; 34:474–479. [PubMed: 21780238]
30. Heaton JM. The distribution of brown adipose tissue in the human. J Anat. 1972; 112:35–39. [PubMed: 5086212]
31. Tanuma Y, Tamamoto M, Ito T, Yokochi C. The occurrence of brown adipose tissue in perirenal fat in Japanese. Arch Histol Jpn. 1975; 38:43–70. [PubMed: 1200786]
32. Gelfand MJ, O'Hara SM, Curtwright LA, Maclean JR. Pre-medication to block ^{18}F-FDG uptake in the brown adipose tissue of pediatric and adolescent patients. Pediatr Radiol. 2005; 35:984–990. [PubMed: 15988582]
33. Söderlund V, Larsson SA, Jacobsson H. Reduction of FDG uptake in brown adipose tissue in clinical patients by a single dose of propranolol. Eur J Nucl Med Mol Imaging. 2007; 34:1018–1022. [PubMed: 17225118]
34. Au-Yong IT, Thorn N, Ganatra R, Perkins AC, Symonds ME. Brown adipose tissue and seasonal variation in humans. Diabetes. 2009; 58:2583–2587. [PubMed: 19696186]
35. Chalfant JS, Smith ML, Hu HH, et al. Inverse association between brown adipose tissue activation and white adipose tissue accumulation in successfully treated pediatric malignancy. Am J Clin Nutr. 2012; 95:1144–1149. [PubMed: 22456659]
36. Kelly DP. Irisin, light my fire. Science. 2012; 336:42–43. [PubMed: 22491843]
37. Boström P, Wu J, Jedrychowski MP, et al. A PGC1-α-dependent myokine that drives brown-fat-like development of white fat and thermogenesis. Nature. 2012; 481:463–468. [PubMed: 22237023]
38. Gilsanz V, Chung SA, Jackson H, Dorey FJ, Hu HH. Functional brown adipose tissue is related to muscle volume in children and adolescents. J Pediatr. 2011; 158:722–726. [PubMed: 21168855]

39. van der Veen DR, Shao J, Chapman S, Leevy WM, Duffield GE. A diurnal rhythm in glucose uptake in brown adipose tissue revealed by in vivo PET-FDG imaging. Obesity (Silver Spring). 2012; 20:1527–2529. [PubMed: 22447290]

40. Chebrolu VV, Hines CD, Yu H, et al. Independent estimation of T2* for water and fat for improved accuracy of fat quantification. Magn Reson Med. 2010; 63:849–857. [PubMed: 20373385]

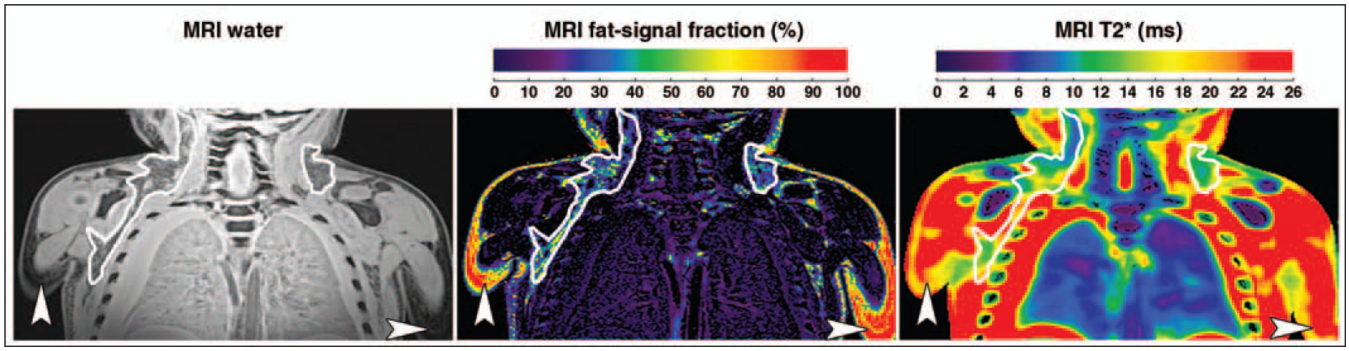

Fig. 1.

Coronal MRI results from 3-year-old boy postmortem. Gray-scale water image (*left*), fat-signal fraction map (*middle*), and T2* map (*right*) illustrate bilateral brown adipose tissue (BAT) depots (*outlines*) and subcutaneous white adipose tissue (WAT) (*arrowheads*). Fat-signal fraction is illustrated using full 0–100% scale. The T2* map is illustrated using scale condensed from 0 to 26 ms for clarity; any tissue with computed T2* value ≥ 26 ms is shown in red. Compared with subcutaneous WAT, note that BAT is characterized by brighter signal and more heterogeneous and granular appearance on water image, lower fat-signal fractions, and slightly shorter T2* values.

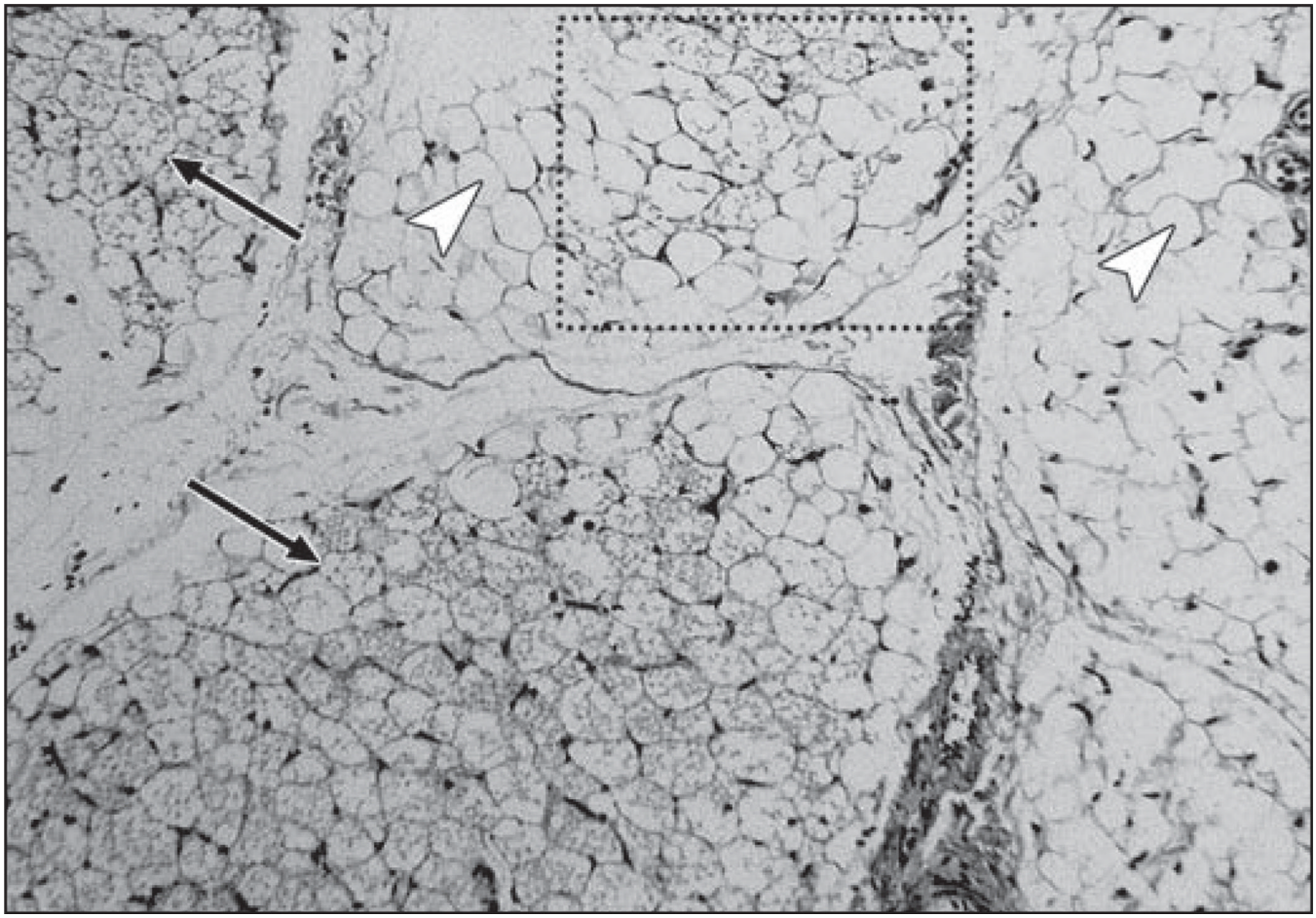

Fig. 2.
Photomicrograph from histologic specimen (H and E, ×10) in 3-year-old boy postmortem (same as in Fig. 1). White arrowheads point to large white adipocytes, each characterized by single intracellular vacuole of triglycerides. In contrast, black arrows point to brown adipocytes, which are smaller and exhibit multiple intracellular triglyceride vacuoles. Dotted box shows area where BAT and WAT adipocytes are intermixed.

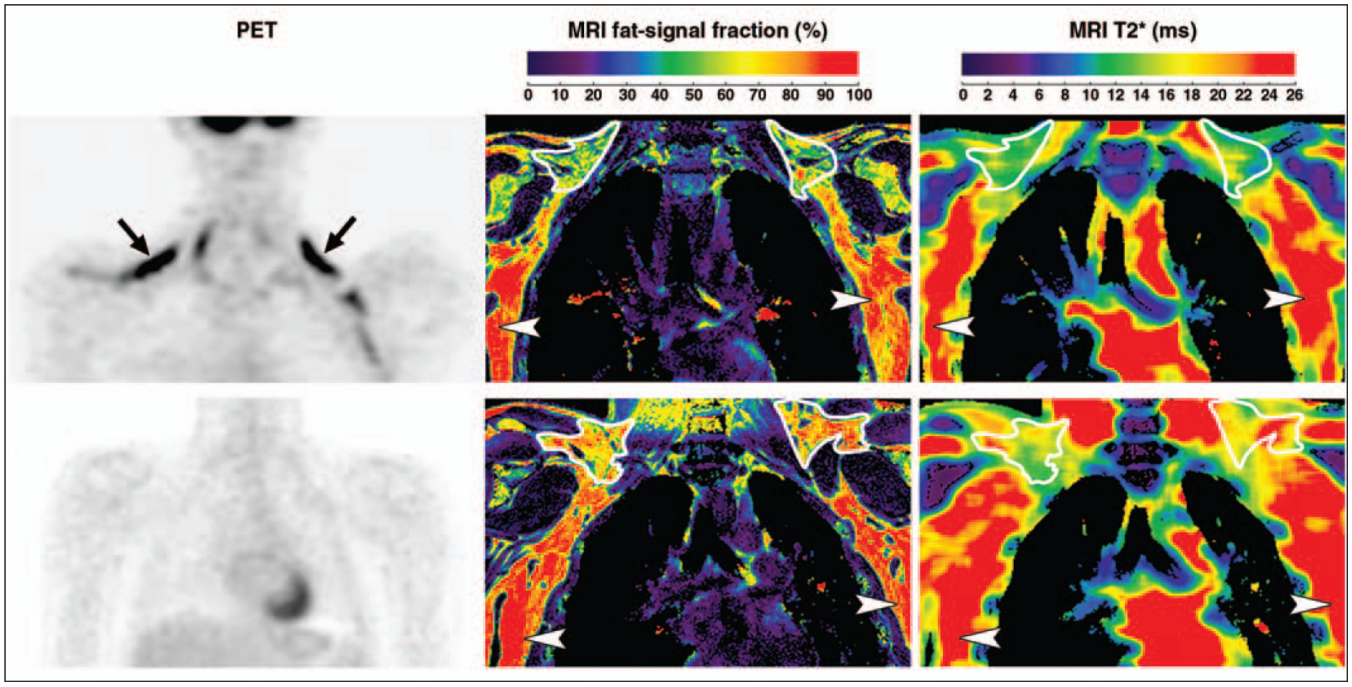

Fig. 3.

Imaging results from adolescent patients 2 and 3. In patient 2, 18-year-old woman who was brown adipose tissue–positive (BAT+) (*top row*), PET data (*left*) highlight evident uptake of radionuclide tracer by BAT (*arrows*). Fat-signal fraction (*middle*) and T2* (*right*) maps from chemical-shift water-fat MRI are shown. BAT (*outlines*) is characterized by lower fat-signal fraction and T2* values in contrast with lipid-rich subcutaneous white adipose tissue (WAT) (*arrowheads*). In patient 3, 18-year-old man who was BAT− (*bottom row*), PET data show no evident uptake of radionuclide tracer by BAT. However, fat-signal fraction and T2* maps show consistently lower values for BAT (*outlines*) than subcutaneous WAT (*arrowheads*).

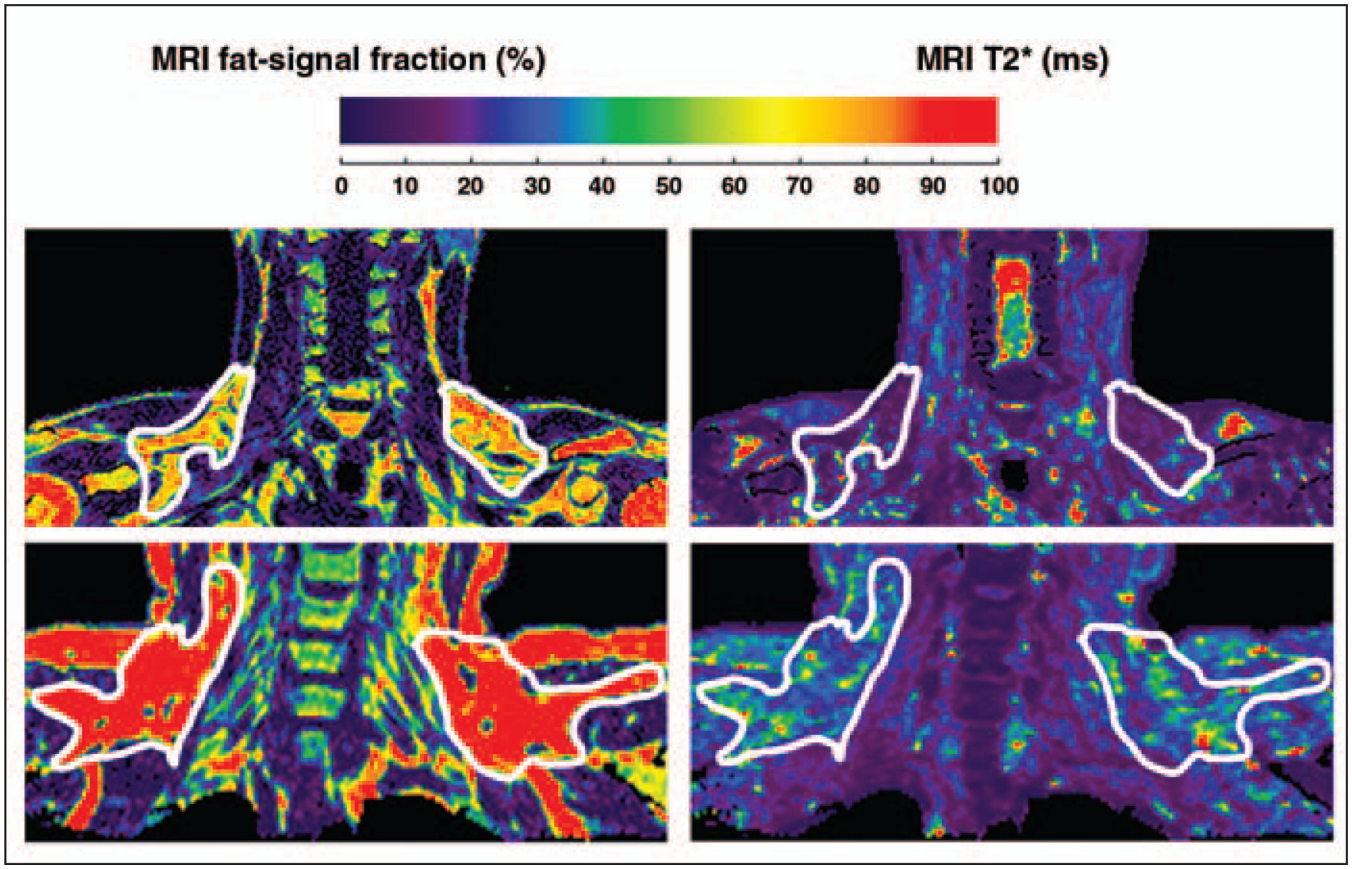

Fig. 4.

Imaging results from adult patient 4, 26-year-old man who was brown adipose tissue–positive (BAT+), and patient 5, 49-year-old woman who was BAT−. PET results are not shown. Fat-signal fraction (*left*) and T2* (*right*) color maps are shown using same nominal 0–100 scale to highlight differences. Scale selection is arbitrary and was chosen for visual clarity. Supraclavicular and interscapular fat pads exhibit lower fat-signal fractions and T2* values in patient 4 (lean) versus patient 5 (moderately overweight). Particularly in patient 5, imaging appearance of BAT depots appears similar to neighboring subcutaneous white adipose tissue.

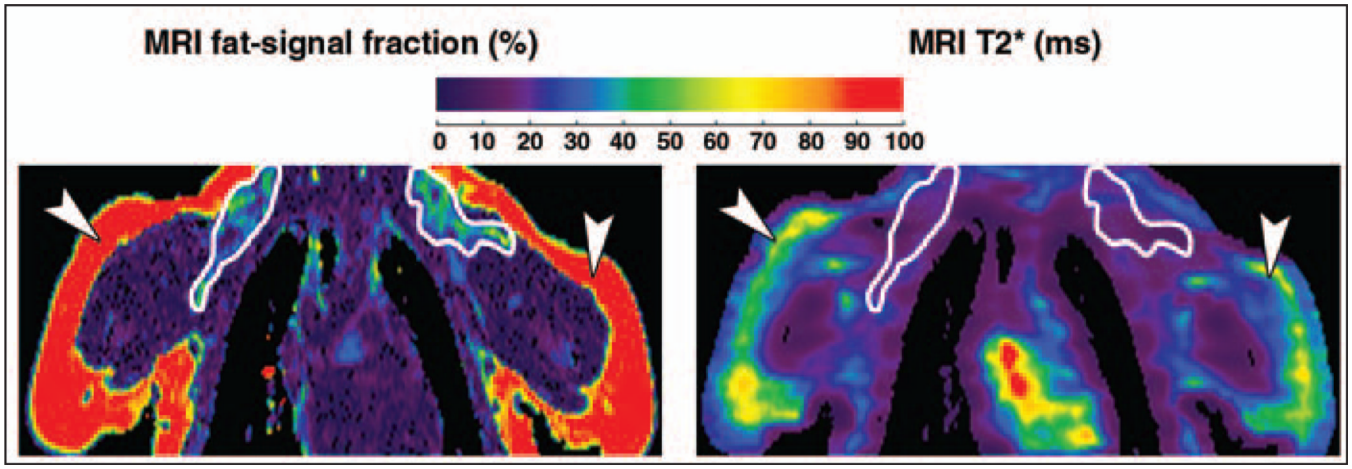

Fig. 5.

Representative imaging results from pediatric patients. In patient 6, 4-month-old boy, lower fat-signal fraction (*left*) and T2* (*right*) values of brown adipose tissue (*outlines*) are evident in comparison with subcutaneous white adipose tissue (*arrowheads*). Similar results were obtained from patients 7 and 8 who were 3 months and 5 years old, respectively.

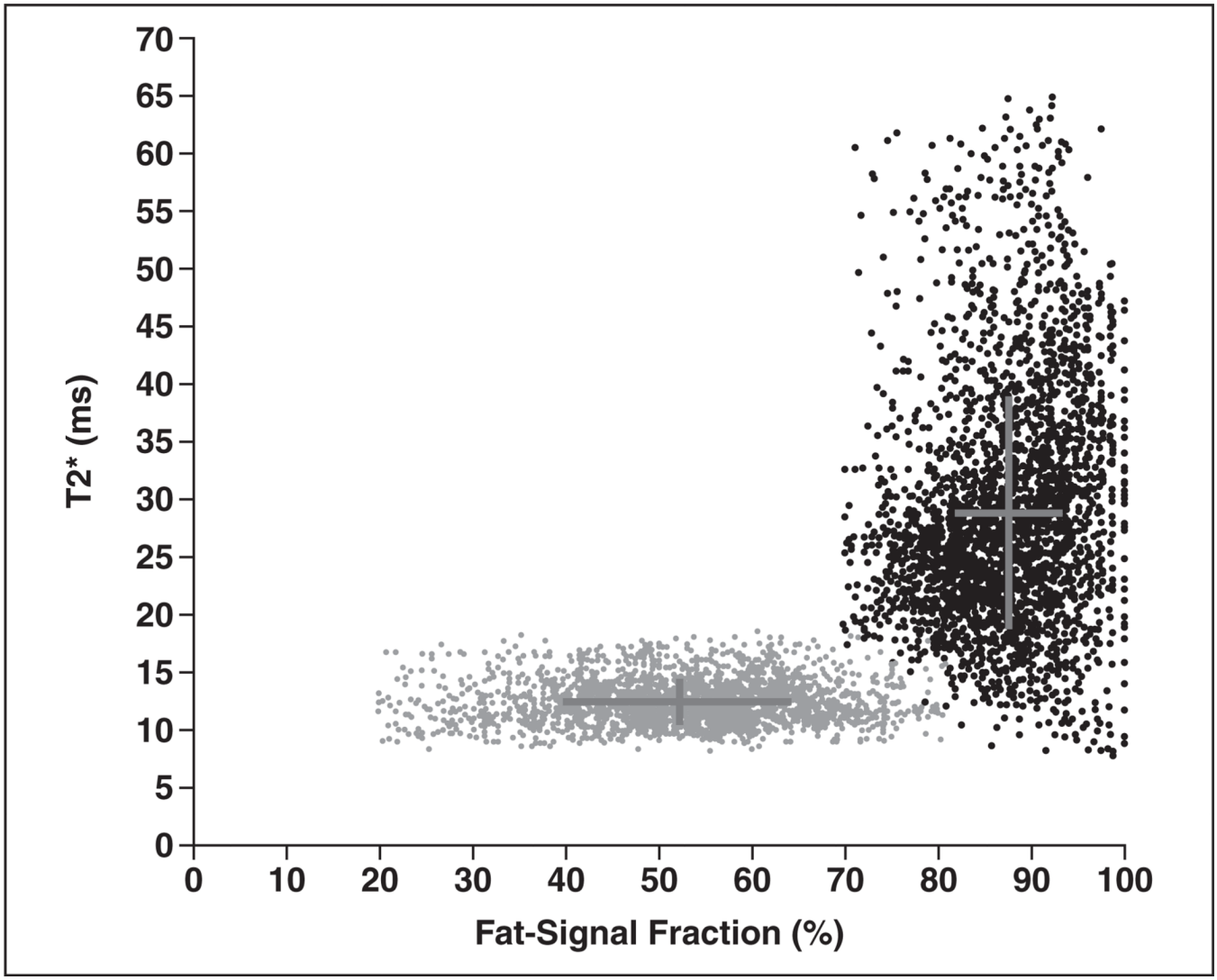

Fig. 6.

Voxel scatterplot graph shows fat-signal fraction and T2* region-of-interest measurements from brown adipose tissue (BAT) (*gray*) and white adipose tissue (WAT) (*black*) for patient 2. Crosses pinpoint means and reflect SD of each distribution along both nominal dimensions. It is evident that BAT occupies distribution with lower fat-signal fraction and T2* values than WAT.

TABLE 1

Characteristics of Study Cohort

Patient No.	Age	Sex	Fat-Signal Fraction (%)		T2* (ms)	
			BAT	WAT	BAT	WAT
Postmortem body	3 y	Boy	29.7 (9.4)	89.8 (5.2)	14.7 (3.4)	21.6 (3.3)
1	18 y	Woman	80.6 (8.9)	91.3 (4.5)	19.4 (3.2)	35.0 (10.1)
2	18 y	Woman	52.0 (12.2)	87.4 (6.3)	12.5 (2.0)	28.8 (10.1)
3	18 y	Man	74.0 (10.5)	89.1 (5.3)	16.9 (3.1)	33.8 (11.1)
4	26 y	Man	66.9 (14.4)	82.8 (8.2)	19.4 (6.8)	40.1 (15.5)
5	49 y	Woman	93.9 (6.8)	95.4 (2.2)	33.4 (8.5)	33.1 (4.8)
6	4 mo	Boy	39.2 (4.1)	92.5 (3.8)	18.6 (4.2)	43.9 (13.3)
7	3 mo	Girl	53.8 (4.0)	92.7 (3.1)	18.4 (4.3)	44.4 (14.5)
8	5 y	Girl	72.5 (4.3)	96.0 (4.2)	20.6 (6.4)	44.7 (9.5)

Note—With the exception of patient 5, all comparisons between brown adipose tissue (BAT) and white adipose tissue (WAT) are statistically significant ($p < 0.05$). Data are average with SD in parentheses.

AJR Am J Roentgenol. Author manuscript; available in PMC 2013 February 05.

TABLE 2

Typical MRI Protocol Parameters for mDIXON Water-Fat Imaging Sequence Used in This Article

Parameter	Value
Pulse sequence	mDIXON, 3D spoiled gradient-echo, cartesian acquisition
Postprocessing	Seven-peak spectral model of fat, monoexponential T2* fit
Coil	16-channel torso array
Orientation	Coronal, head first, supine
TR (ms)	9–13
First TE / echo spacing (Δ TE) (ms)	1.2–1.4 / 1.0–1.2
Number of echoes	6
Flyback echoes	No
Frequency axis	Superior/inferior
Phase axis	Right/left
Spatial resolution (mm)	1 × 1
No. of slices	100–150
Acquired slice thickness (mm)	2 (overlapping)
Reconstructed slice thickness (mm)	1
Flip angle	3°
Bandwidth (kHz/pixel)	1.3
Parallel imaging acceleration	2
No. of signal averages	1

Note—mDIXON manufactured by Philips Healthcare.